

# Improving Molecular Modeling with Geometric GNNs: an Empirical Study

Ali Ramlaoui<sup>\*12</sup> Théo Saulus<sup>\*12</sup> Basile Terver<sup>\*32</sup>  
 Victor Schmidt<sup>456</sup> David Rolnick<sup>57</sup> Fragkiskos D. Malliaros<sup>18</sup> Alexandre Duval<sup>1856</sup>

## Abstract

Rapid advancements in machine learning (ML) are transforming materials science by significantly speeding up material property calculations. However, the proliferation of ML approaches has made it challenging for scientists to keep up with the most promising techniques. This paper presents an empirical study on Geometric Graph Neural Networks for 3D atomic systems, focusing on the impact on performance, scalability, and symmetry enforcement of different (1) canonicalization methods, (2) graph creation strategies, and (3) auxiliary tasks. Our findings and insights aim to guide researchers in selecting optimal modeling components for molecular modeling tasks. Our code is available at <https://github.com/RolnickLab/ocp>.

## 1. Introduction

The field of computational materials science has witnessed an increasing interest in recent years, with the explosion of machine learning approaches to model material properties at the quantum scale. This is possible thanks to the release of large-scale datasets such as OC20 (Chanussot et al., 2020) and QM7-X (Hoja et al., 2021), which contain millions of molecular structures along with various properties (forces, energy, band gap) computed using quantum mechanical simulations involving Density Functional Theory (DFT) (Kohn et al., 1996).

ML models have been trained to approximate DFT, thus constituting an even faster proxy to the Schrödinger equation, modeling atomic interactions and systems' behavior.

<sup>\*</sup>Equal contribution <sup>1</sup>Université Paris-Saclay, Centrale-Supélec <sup>2</sup>École Normale Supérieure Paris-Saclay <sup>3</sup>École Polytechnique, IP Paris <sup>4</sup>Université de Montréal <sup>5</sup>Mila - Quebec AI Institute <sup>6</sup>Entalpic <sup>7</sup>McGill University <sup>8</sup>Inria Saclay. Correspondence to: Ali Ramlaoui <ali.ramlaoui@student-cs.fr>, Théo Saulus <theo.saulus@student-cs.fr>, Basile Terver <basile.terver@polytechnique.edu>.

Accepted at the 1st Machine Learning for Life and Material Sciences Workshop at ICML 2024. Copyright 2024 by the author(s).

They enable the calculation of material properties in seconds instead of hours or days, offering the potential to accelerate scientific discovery via high-throughput screening of novel materials (Batatia et al., 2023a; Merchant et al., 2023). However, the explosion of ML approaches in recent years makes it hard to keep up with promising techniques for scientists in the field. While some surveys have attempted to structure the different categories of ML approaches (Han et al., 2022; Duval et al., 2024), these do not focus on empirical evaluation.

In this paper, we propose an empirical study of some key modeling aspects of Geometric GNNs for 3D atomic systems. Specifically, we investigate the impact of 1) the recent canonicalization methods used to enforce or approximate Euclidean symmetries, 2) the graph creation step when modeling a 3D atomic system, and 3) adding several auxiliary tasks. We focus on the OC20 dataset modeling the relaxed adsorption energy of an adsorbate-catalyst system. We hope that the conclusions and insights drawn from our experiments will benefit the community, making it possible to quickly choose the right modeling component.

## 2. Choice of Canonicalization

A function  $f : \mathcal{X} \rightarrow \mathcal{X}$  is said to be equivariant with respect to a transformation  $t$  if  $\forall x \in \mathcal{X}, f(t(x)) = t(f(x))$ . In particular,  $f$  is  $E(3)$ -equivariant if it is equivariant to rotations, translations, and reflections.  $E(3)$ -equivariance is a desirable property in molecular modeling to learn representations that are best suited for physically meaningful tasks, such as force predictions on atoms (e.g., S2EF task of OC20). This can be enforced in the architecture of the model during the message passing steps by using equivariant features of the input's representation (Schütt et al., 2021; Batatia et al., 2023b; Liao & Smidt, 2023), which comes at the cost of expensive feature computations. A recent alternative to these equivariant architectures lies in unconstrained GNNs, which do not enforce  $E(3)$ -equivariance by model design but instead with a coordinate-preprocessing step referred to as canonicalization (Hu et al., 2021; Duval et al., 2023; Pozdnyakov & Ceriotti, 2024). This process grants unconstrained GNNs with greater flexibility, scalability, and often expressivity (Duval et al., 2024). Commonly, it involves

projecting (e.g., with PCA or an equivariant network) the input atomic system into a canonical space such that every Euclidean transformation of the same system gets mapped to the same canonical representation, i.e. handling symmetries in the data pre-processing.

Since these canonicalization methods are all recent and no comparison has yet been drawn, we benchmark the proposed approaches on QM9 and OC20 tasks, evaluating their impact on performance and symmetry enforcement.

### 2.1. Canonicalization for direct predictions

In this subsection, we evaluate several canonicalization procedures with the FAENet backbone architecture (Duval et al., 2023), a powerful unconstrained GNN which is not equivariant by itself. We assume familiarity of the reader with these approaches but provide a description in Appendix A.

- Vector Neurons Network (VNN) (Deng et al., 2021) using the VN re-implementation of PointNet (Qi et al., 2017) and DGCNN (Wang et al., 2019). This class of canonicalization networks is  $SO(3)$ -equivariant by design and is applied to obtain a canonical representation of the data following the method of Kaba et al. (2023).
- Stochastic Frame Averaging (SFA) (Duval et al., 2023), designed to avoid averaging the predictions over 8 elements of the frame as required by Frame Averaging (Puny et al., 2021). Instead, we sample one canonical orientation at random at each epoch, similar to data augmentation on a small and complete set.
- A novel method denoted SFA+SignNet, where we propose to map the several projection matrices of SFA to a single one using a sign-equivariant network proposed in SignNet (Lim et al., 2023b;a). The rationale is to handle the sign ambiguity problem of PCA that exists in SFA with a small dedicated network to get a unique canonical representation of Euclidean transformations. We propose two implementations of SignNet, either using VNNs to have a perfect  $E(3)$ -equivariance when combined with SFA or using MLPs without theoretical guarantees.

For VNNs and SFA+SignNet methods, we test both training and freezing the weights of the Canonicalization Network (CN). We report performance on the OC20 IS2RE, OC20 S2EF, and QM9 in Tables 1, 5, 6, 7, 8, and 9.

In our OC20 IS2RE experiment, we found there are almost no differences between the various canonicalization methods, with MAE of 594, 598, and 593 for SFA, VN-PointNet, and VN-DGCNN. Specially, non-exact canonicalizations (SFA and SFA+SignNet) demonstrate equal or

Canonicalization	Cano. trained parameters	avg. MAE (meV) ↓	EwT (ID) (%) ↑	3D Rotation Invariance ↓
SFA	0	594	4.40	$1.30 \cdot 10^{-2}$
(U) SFA+MLP-SignNet	0	<b>580</b>	4.48	$9.71 \cdot 10^{-2}$
(T) SFA+MLP-SignNet	454	583	4.46	$4.00 \cdot 10^{-2}$
(U) SFA+VN-SignNet	0	592	<b>4.69</b>	$7.58 \cdot 10^{-3}$
(T) SFA+VN-SignNet	2,620	599	4.25	$2.57 \cdot 10^{-2}$
(U) VN-Pointnet	0	605	4.09	$4.62 \cdot 10^{-3}$
(T) VN-Pointnet	1,310	598	4.12	<b><math>3.80 \cdot 10^{-3}</math></b>
(U) VN-DGCNN	0	600	4.31	$3.11 \cdot 10^{-2}$
(T) VN-DGCNN	663,804	593	4.42	$9.10 \cdot 10^{-3}$

Table 1. Invariance comparison of canonicalization methods on OC20 IS2RE dataset. (U) (resp. (T)) indicates an untrained (resp. trained) canonicalization network. FAENet backbone has 4,147,731 parameters. More details in Tables 5 and 6.

better MAE than perfectly equivariant methods (e.g., VN-based). This suggests that heuristics approximation of equivariance should be sufficient in some practical applications like OC20. This is aligned with what Duval et al. (2023) suggested when showing that SFA outperforms exact Frame Averaging in terms of downstream performance.

In terms of symmetry enforcement, non-exact methods are surprisingly nearly as effective as fully invariant methods, suggesting that the FAENet backbone implicitly learns to handle symmetries.

Regarding exact canonicalization methods, we observe that training or not the network and swapping one method for another has little impact on model performance. This tends to indicate that the canonical networks’s ability to introduce equivariance is more critical than the choice of the canonicalization method.

### 2.2. Canonicalization for relaxed IS2RE

Previous work showed that solving the IS2RE task yields better results by performing relaxed energy predictions rather than direct energy estimation (Liao et al., 2023). Here, we evaluate whether canonicalization methods also perform well at relaxing a trajectory. Table 2 reports the performances of FAENet with multiple symmetry-preserving methods, with the invariant SchNet model and direct IS2RE acting as baseline. Our findings suggest that relaxed IS2RE predictions are competitive with direct IS2RE predictions and are interesting directions to explore for improving molecular property predictions with these architectures. Moreover, a potential explanation as to why the relaxations do not yield significant improvements over direct IS2RE may involve the approximate equivariance or the lack of continuity in some of these canonicalization methods, as pointed out in Dym et al. (2024), which may hamper accurate and smooth relaxations trajectories. This is mainly true for SFA, where a frame is randomly picked at each step of the relaxation, meaning that the canonical inputs can also be far from each other. Lastly, note that exact equivariant meth-

Model	IS2RE		IS2RS	
	EwT (%) $\uparrow$	MAE (eV) $\downarrow$	DwT (%) $\uparrow$	Pos. MAE $\downarrow$
FAENet (Direct)	4.05	0.551	-	-
FAENet (SFA)	4.92	0.587	31.1	0.390
FAENet (UTPN)	5.64	0.560	33.7	0.381
SchNet	1.89	0.912	15.0	0.461

Table 2. Results on the IS2RE and IS2RS tasks for the VAL-ID validation dataset of OC20 using iterative relaxations. The S2EF models’ results are reported in Appendix A.5. Note that these results can only be obtained by keeping the tag 0 atoms of the subsurface as they are important for relaxations.

ods for relaxed IS2RE predictions such as the untrained VN-PointNet (UTPN) implementation from (Kaba et al., 2023) yields better MAE than the approximate equivariance module SFA. Still, during our experiments we found that with further focus on the accuracy of S2EF models, canonicalization methods used to enforce symmetries can become more appealing using iterative relaxation methods.

### 3. Graph Creation Study

For large molecular structures, electrostatic long-range interactions are non-negligible components of the system’s dynamics (Gasteiger et al., 2019). While various methods have tried to model long-range interactions between far-away atoms, they often suffer from the over-smoothing effect when increasing the number of interaction layers (Liao & Smidt, 2023). As a result, models where the geometric graph is modelled using a cutoff distance between neighbour atoms have been shown to work best. Since properly handling these interactions is essential to accurately simulate the system, we explore in this section the impact of this creation step and the rewiring strategies.

#### 3.1. Graph cutoff and rewiring

First, we vary the cutoff distance<sup>1</sup> used during the creation of the graph to check whether linking more atoms with each other helps in learning these couplings. We report the results for the FAENet model on the OC20 IS2RE task in Table 3.

A small cutoff of 1.0 Å leads to the weakest performance, which makes sense since the associated graph is almost empty and nodes are isolated, i.e. messages can not pass correctly. A large cutoff or a complete graph also leads to poor performance despite every atomic interaction being modeled. Within an intermediary range of cutoff values, the model achieves optimal learning with computational efficiency. This is in accordance with past observations where the locality bias of GNN models seemed to fit really well with atomic system property prediction tasks. Thus,

<sup>1</sup>When representing the 3D point cloud with a graph, we create an edge between any two atoms if their are within a fixed cutoff distance, and no edge otherwise.

Model	ID	
	EwT (%) $\uparrow$	MAE (eV) $\downarrow$
Cutoff 30 - Max neighbours 40	2.65	0.697
Cutoff 20 - Max. neighbours 40	3.08	0.673
Cutoff 20 - Max. neighbours 10	2.25	0.768
Cutoff 10 - Max. neighbours 50	4.17	0.553
Cutoff 10 - Max. neighbours 10	4.49	0.553
Cutoff 6 - Max. neighbours 40	4.31	0.553
Cutoff 1 - Max. neighbours 40	1.35	1.069

Table 3. Impact of the cutoff on the performance of FAENet on the OC20 IS2RE task. Full Table in Appendix B.1.

although the creation of the graph through a well-chosen cutoff is important, the margin for fine-tuning this parameter is large enough.

The fact that better graphs are adapted to GNN functioning rather than the precise modeling of the situation, where all atoms interact with each other, echoes what Duval et al. (2022) have stated. Indeed, they showed that to fit the GNN message passing scheme, removing repeating subsurface atoms of the adsorbate did not affect the model performance on IS2RE tasks. Similarly to having a moderate cutoff, the performance improvements of such a strategy are decisive for scalability. As an empirical example, we tried to run an EquiformerV2 (Liao et al., 2023) model for IS2RE with the remove-tag-0 method on an 80GB A100 GPU, leading to a 5 $\times$  speed-up with no performance loss and proving the relevance of this technique even on very large models.

#### 3.2. Ewald-based long range message passing

Since a small value for the cutoff seems to be the most interesting one, we want to model the long interactions differently than adding links between all atoms. Ewald-based Message Passing (EMP) (Kosmala et al., 2023) is introduced in this perspective. It incorporates a physics-based prior in the architecture to model the long-range electrostatic potential via a nonlocal Fourier space scheme, drawing edges based on a cutoff on frequency instead of distances.

Our experiments, given in Table 4, show that EMP is interesting for an invariant method like SchNet (Schütt et al., 2017), which limits its geometric information to atom pairwise distances. However, EMP does not benefit more advanced GNNs like FAENet. To understand why, we plot in Figure 1 the cosine similarity between the embeddings throughout interaction layers. We observe that SchNet and FAENet learn very different representations. Indeed, while the representation of each atom in SchNet tends to be similar to nearby atoms, FAENet is able to give very different embeddings for them. A potential explanation could be that because FAENet is a more expressive model, the propagated messages are less constrained and thus can lead to very diverse atom representations without Ewald. On the other hand, embeddings of SchNet only become diversified

Model	ID	
	EwT (%) $\uparrow$	MAE (eV) $\downarrow$
FAENet (Graph Rewiring)	4.05	0.551
FAENet (Graph Rewiring) + Ewald	4.12	0.562
FAENet (No Graph Rewiring)	4.54	0.544
FAENet (No Graph Rewiring) + Ewald	4.11	0.556
SchNet (Graph Rewiring)	3.18	0.641
SchNet (Graph Rewiring) + Ewald	3.54	0.604
SchNet (No Graph Rewiring)	2.93	0.654
SchNet (No Graph Rewiring) + Ewald	3.48	0.597

Table 4. Comparison of the performances of FAENet and SchNet with and without Ewald Message Passing on the IS2RE task. Full table and results for the QM9 dataset in Appendix B.2.

using Ewald, maybe because incorporating longer messages helps create more distinct representations. More plots can be found in Appendix B.2. One interesting takeaway is that EMP helps take into account long-range interactions for simple models and GNNs with symmetry-constrained layers (Kosmala et al., 2023) but is less efficient on expressive models.

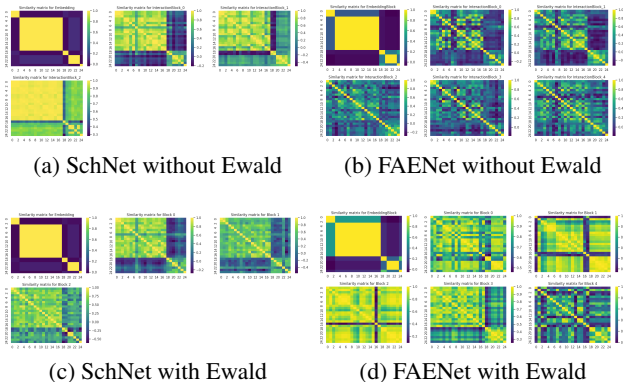


Figure 1. Similarity matrix of the embeddings of the atoms of a randomly picked system for different interaction blocks from the training set of OC20. The same system is used every time to be able to compare the different results.

## 4. Auxiliary Tasks

In this section, we study how to leverage other tasks to improve the performance of FAENet on IS2RE.

### 4.1. Noisy nodes IS2RS auxiliary task

First, we recall that increasing the number of interaction blocks above 8 does not yield better performance for most geometric GNNs, with a dramatic loss of information after 14 layers in the classical FAENet IS2RE setup, as illustrated in Table 14. To address the oversmoothing issue, Godwin et al. (2022) propose to use noisy regularisation, introducing their method called Noisy Nodes. It consists of adding an auxiliary node-level denoising task that encourages diversity

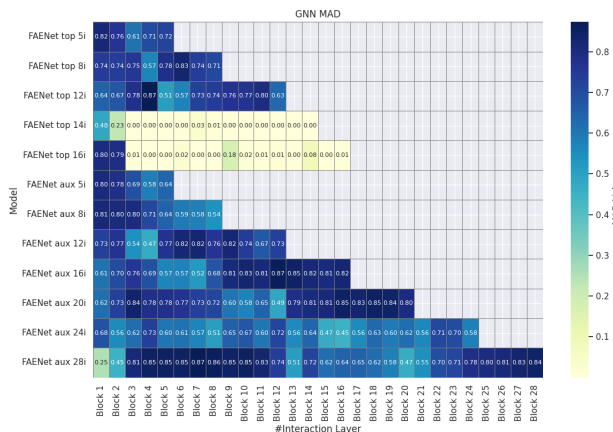


Figure 2. MAD values of the graph embeddings (averaged over 50 randomly sampled graphs of the train set) throughout the interaction layers for various models. “FAENet top” models are trained with the top configs of the classical FAENet model (Duval et al., 2023) but with more epochs and lower batch size (128). “FAENet aux” models are our models trained on IS2RE with IS2RS auxiliary task. A model having xx interaction layers is indicated as “XXi”.

in the latent representations of the nodes (more details in C.2).

Here, we implement Noisy Nodes for the IS2RE task, which is done by adding a position decoding head running in parallel to the original energy prediction head. Our implementation takes inspiration from other state-of-the-art models such as EquiformerV1 (Liao & Smidt, 2023), which benefit from using Noisy Nodes on the IS2RE task (more details in C.2).

To understand the reason for the performance drop for the classical FAENet IS2RE setup of (Duval et al., 2023) when adding interaction layers in Table 14, we plot the Mean Average Distance (MAD) (Chen et al., 2019), averaged over 50 input adsorbate-catalyst pairs, of their embeddings throughout the interaction blocks in Figure 2. The classical FAENet models (“FAENet top”) with 14 interaction layers or more see their latent node representations all collapse to almost the same vector, since the MAD goes to almost zero as we go deeper in the model’s interaction layers, which is a manifestation of oversmoothing. Figure 2 shows that the models trained with Noisy Nodes IS2RS auxiliary task (“FAENet aux”) do not suffer from oversmoothing (i.e. MAD going to zero) even when going as deep as 28 interaction layers.

Then, we compare the performances of our new FAENet models trained on IS2RE Noisy Nodes, varying the number of interaction layers, as summarized in Table 15. First, we observe a clear correlation between the performances and the number of blocks. Second, the best model trained with Noisy Nodes, which has 26 interaction blocks, outperforms

the best models of (Duval et al., 2023), allowing the average MAE to decrease from 568 meV to 525 and the average EwT percentage to increase from 3.78% to 4.43%. Details about our experimental setup are given in Appendix C.1. We observe that the throughput at inference is divided by two between the smallest (5 interaction layers) and biggest model (28 layers). The best tradeoff seems to be around 16 interaction layers, similar to what (Liao & Smidt, 2023) choose for their models trained with IS2RS auxiliary task.

The current most general state-of-the-art models for atomic property prediction, such as (Shoghi et al., 2024) only make use of backbone GNNs (such as GemNet-OC (Gasteiger et al., 2022)) with not more than 6 interaction blocks. Noisy Nodes proves to be a regularisation technique that can be used across models, having equivariant (Liao & Smidt, 2023) or non-equivariant (Duval et al., 2023) features, to leverage the power of more interaction layers and improve performance. On direct IS2RE, our experiments only show a slightly increasing performance with the number of blocks. Yet, unlocking the potential of deeper GNNs with this simple regularisation allows greater freedom in training or pretraining on larger datasets or for more complex tasks, such as relaxed IS2RE 2.2. Our focus for FAENet was on IS2RE, but we expect similar results on S2EF, IS2RS, and other datasets such as QM9 or QM7-X, as obtained by (Godwin et al., 2022) with other GNNs such as GNS (Sanchez-Gonzalez et al., 2020).

#### 4.2. Learning equivariance with more interaction layers

As previously stated, equivariant networks are preferred when handling 3D point clouds. However, in the field of protein structure prediction, we were caught by the AlphaFold3 architecture (Abramson et al., 2024) that chose non-equivariant networks in its diffusion module, contrary to AlphaFold2 (Jumper et al., 2021). Thus, we tested whether a deep GNN with no equivariance enforced could learn the equivariance from the data and match performances with canonicalized models using the FAENet backbone, as in Section 2.

We compare our models trained on IS2RE with IS2RS auxiliary task in two settings: with SE(3)-SFA and without any canonicalization method (No-FA). The results are displayed in Table 16. They reveal that, even with many additional interaction blocks (up to 26), both the MAE and the equivariance property do not improve compared to using SE(3)-SFA, meaning that imposing equivariance is still a beneficial inductive bias. Unfortunately, in our setting, having a deeper network does not allow to learn invariance and equivariance more effectively. Further analysis would be needed with larger datasets and other methods to reinforce this argument or find its limits (if any).

#### 4.3. Pre-training on different tasks

With the release of larger datasets, the community has increasingly shifted towards pre-training and transfer learning approaches (Batatia et al., 2023a; Shoghi et al., 2024; Deng et al., 2023). We make a step in this direction in this subsection by pre-training our model on the S2EF, which contains roughly two orders of magnitude more data points, and by fine-tuning it on IS2RE, hoping to transfer some knowledge of atomic interactions. More precisely, we leverage the extensive S2EF dataset to utilize all trajectories while maintaining high inference throughput by performing direct energy predictions. Although training on S2EF is more time-consuming than on IS2RE, separating the learning of relaxation and molecular interactions may yield better results than training IS2RE directly from scratch.

Figure 7 in Appendix C.6 shows that with this approach, the energy MAE starts at a better value during training but evolves much slower and converges to a slightly better result (0.53 eV vs. 0.55 eV on the validation ID split). This shows that while the model starts with a good representation of molecular dynamics, the differences are not significant because dynamics are not taken into account by the S2EF training process. Learning molecular interactions through auxiliary tasks with or without dynamics is helpful to achieve better performances, but this pre- or joint training needs to be correctly incorporated into the architecture so as not to overwrite the learned information during the downstream task. This opens the way for new architectures designed to leverage materials design knowledge between tasks and datasets (Shoghi et al., 2024). Whether by training with auxiliary tasks or on other datasets, there seems to be transfer learning and generalization capabilities in atomic property prediction, as in NLP. Hence, we recommend to further explore this promising area of research.

## 5. Conclusion

In this study, we explored various techniques aimed at enhancing the performance of geometric GNNs for molecular modeling. Our empirical study covered several aspects, with the main observations being summarized below.

**Canonicalization methods.** While exact methods provide the best theoretical guarantees for equivariance, approximate heuristics such as SFA seem to yield better performance. This opens questions about how to design canonicalizations that are the most effective in practice, beyond theoretical guarantees, and leaves a broader set of possibilities for the model design, too.

**Graph creation.** Although accurate graph construction is important, many viable options can be considered without significant differences in performance. Furthermore,

physics-inspired modules such as Ewald-based message passing demonstrate improved performance for symmetry-constrained models such as SchNet but do not provide any benefits to more expressive models such as FAENet.

**Auxiliary tasks.** Implementing Noisy Nodes as an auxiliary task significantly enhances the performance of FAENet by leveraging the benefits of much deeper GNNs. As with pretraining on different tasks such as S2EF, there is evidence of transfer learning for atomic property prediction, and we recommend more exploration of this path in the flavor of (Shoghi et al., 2024).

Future work could focus on refining these techniques, exploring their applications across a wider spectrum of datasets, and developing new methods to combine the strengths of various approaches.

## Acknowledgement

The authors thank Sékou-Oumar Kaba, Derek Lim, Joshua David Robinson, and Hannah Lawrence for their insightful comments and discussions, as well as the anonymous reviewers for their suggestions and feedback. Supported in part by ANR (French National Research Agency) under the JCJC project GraphIA (ANR-20-CE23-0009-01) and the Canada CIFAR AI Chairs program. This research was enabled in part by computing resources provided by Mila (mila.quebec) and material support from NVIDIA Corporation in the form of computational resources.

## References

- Abramson, J., Adler, J., Dunger, J., Evans, R., Green, T., Pritzel, A., Ronneberger, O., Willmore, L., Ballard, A. J., Bambrick, J., et al. Accurate structure prediction of biomolecular interactions with alphafold 3. *Nature*, pp. 1–3, 2024.
- Batatia, I., Benner, P., Chiang, Y., Elena, A. M., Kovács, D. P., Riebesell, J., Advincula, X. R., Asta, M., Baldwin, W. J., Bernstein, N., et al. A foundation model for atomistic materials chemistry. *arXiv preprint arXiv:2401.00096*, 2023a.
- Batatia, I., Kovács, D. P., Simm, G. N. C., Ortner, C., and Csányi, G. Mace: Higher order equivariant message passing neural networks for fast and accurate force fields, 2023b.
- Chanussot, L., Das, A., Goyal, S., Lavril, T., Shuaibi, M., Rivière, M., Tran, K., Heras-Domingo, J., Ho, C., Hu, W., Palizhati, A., Sriram, A., Wood, B., Yoon, J., Parikh, D., Zitnick, C. L., and Ulissi, Z. W. The open catalyst 2020 (oc20) dataset and community challenges. *ACS Catalysis*, 2020. doi: 10.1021/acscatal.0c04525.
- Chen, D., Lin, Y., Li, W., Li, P., Zhou, J., and Sun, X. Measuring and relieving the over-smoothing problem for graph neural networks from the topological view, 2019.
- Deng, B., Zhong, P., Jun, K., Riebesell, J., Han, K., Bartel, C. J., and Ceder, G. Chgnet: Pretrained universal neural network potential for charge-informed atomistic modeling. *arXiv preprint arXiv: 2302.14231*, 2023.
- Deng, C., Litany, O., Duan, Y., Poulenard, A., Tagliasacchi, A., and Guibas, L. J. Vector neurons: A general framework for so(3)-equivariant networks. In *Proceedings of the IEEE/CVF International Conference on Computer Vision*, pp. 12200–12209, 2021.
- Duval, A., Schmidt, V., Miret, S., Bengio, Y., Hernández-García, A., and Rolnick, D. Phast: Physics-aware, scalable, and task-specific gnn for accelerated catalyst design. *arXiv preprint arXiv: 2211.12020*, 2022.
- Duval, A., Schmidt, V., Garcia, A., Miret, S., Malliaros, F. D., Bengio, Y., and Rolnick, D. Faenet: Frame averaging equivariant gnn for materials modeling. *International Conference on Machine Learning*, 2023. doi: 10.48550/arXiv.2305.05577.
- Duval, A., Mathis, S. V., Joshi, C. K., Schmidt, V., Miret, S., Malliaros, F. D., Cohen, T., Liò, P., Bengio, Y., and Bronstein, M. A hitchhiker’s guide to geometric gnn for 3d atomic systems. 2024.
- Dym, N., Lawrence, H., and Siegel, J. W. Equivariant frames and the impossibility of continuous canonicalization, 2024.
- Gasteiger, J., Groß, J., and Günnemann, S. Directional message passing for molecular graphs. In *International Conference on Learning Representations*, 2019.
- Gasteiger, J., Shuaibi, M., Sriram, A., Günnemann, S., Ulissi, Z., Zitnick, C. L., and Das, A. Gemnet-oc: Developing graph neural networks for large and diverse molecular simulation datasets, 2022.
- Godwin, J., Schaarschmidt, M., Gaunt, A., Sanchez-Gonzalez, A., Rubanova, Y., Veličković, P., Kirkpatrick, J., and Battaglia, P. Simple gnn regularisation for 3d molecular property prediction & beyond, 2022.
- Han, J., Rong, Y., Xu, T., and Huang, W. Geometrically equivariant graph neural networks: A survey. *arXiv preprint arXiv:2202.07230*, 2022.
- Hoja, J., Sandonas, L. M., Ernst, B. G., Vázquez-Mayagoitia, A., Jr., R. A. D., and Tkatchenko, A. Qm7-x: A comprehensive dataset of quantum-mechanical properties spanning the chemical space of small organic molecules. *Scientific Data*, 2021. doi: 10.1038/s41597-021-00812-2.

- Hu, W., Shuaibi, M., Das, A., Goyal, S., Sriram, A., Leskovec, J., Parikh, D., and Zitnick, C. L. Forcenet: A graph neural network for large-scale quantum calculations. *arXiv preprint arXiv: 2103.01436*, 2021.
- Jumper, J., Evans, R., Pritzel, A., Green, T., Figurnov, M., Ronneberger, O., Tunyasuvunakool, K., Bates, R., Žídek, A., Potapenko, A., et al. Highly accurate protein structure prediction with alphafold. *Nature*, 596(7873):583–589, 2021.
- Kaba, S.-O., Mondal, A. K., Zhang, Y., Bengio, Y., and Ravanbakhsh, S. Equivariance with learned canonicalization functions. In *International Conference on Machine Learning*, pp. 15546–15566. PMLR, 2023.
- Kohn, W., Becke, A. D., and Parr, R. G. Density functional theory of electronic structure. *The Journal of Physical Chemistry*, 100(31):12974–12980, 1996.
- Kosmala, A., Gasteiger, J., Gao, N., and Günnemann, S. Ewald-based long-range message passing for molecular graphs. *arXiv preprint arXiv:2303.04791*, 2023.
- Liao, Y.-L. and Smidt, T. Equiformer: Equivariant graph attention transformer for 3d atomistic graphs, 2023.
- Liao, Y.-L., Wood, B., Das, A., and Smidt, T. Equiformerv2: Improved equivariant transformer for scaling to higher-degree representations, 2023.
- Lim, D., Robinson, J., Jegelka, S., and Maron, H. Expressive sign equivariant networks for spectral geometric learning, 2023a.
- Lim, D., Robinson, J. D., Zhao, L., Smidt, T., Sra, S., Maron, H., and Jegelka, S. Sign and basis invariant networks for spectral graph representation learning. In *The Eleventh International Conference on Learning Representations*, 2023b. URL <https://openreview.net/forum?id=Q-UHqMorzil>.
- Merchant, A., Batzner, S., Schoenholz, S. S., Aykol, M., Cheon, G., and Cubuk, E. D. Scaling deep learning for materials discovery. *Nature*, 624(7990):80–85, 2023.
- Pozdnyakov, S. and Ceriotti, M. Smooth, exact rotational symmetrization for deep learning on point clouds. *Advances in Neural Information Processing Systems*, 36, 2024.
- Puny, O., Atzmon, M., Smith, E. J., Misra, I., Grover, A., Ben-Hamu, H., and Lipman, Y. Frame averaging for invariant and equivariant network design. In *International Conference on Learning Representations*, 2021.
- Qi, C. R., Su, H., Mo, K., and Guibas, L. J. Pointnet: Deep learning on point sets for 3d classification and segmentation, 2017.
- Sanchez-Gonzalez, A., Godwin, J., Pfaff, T., Ying, R., Leskovec, J., and Battaglia, P. Learning to simulate complex physics with graph networks. In III, H. D. and Singh, A. (eds.), *Proceedings of the 37th International Conference on Machine Learning*, volume 119 of *Proceedings of Machine Learning Research*, pp. 8459–8468. PMLR, 13–18 Jul 2020. URL <https://proceedings.mlr.press/v119/sanchez-gonzalez20a.html>.
- Schreiner, M., Bhowmik, A., Vegge, T., Busk, J., and Winther, O. Transition1x – a dataset for building generalizable reactive machine learning potentials, 2022.
- Schütt, K., Kindermans, P.-J., Sauceda Felix, H. E., Chmiela, S., Tkatchenko, A., and Müller, K.-R. Schnet: A continuous-filter convolutional neural network for modeling quantum interactions. *Advances in neural information processing systems*, 30, 2017.
- Schütt, K. T., Unke, O. T., and Gastegger, M. Equivariant message passing for the prediction of tensorial properties and molecular spectra, 2021.
- Shoghi, N., Kolluru, A., Kitchin, J. R., Ulissi, Z. W., Zitnick, C. L., and Wood, B. M. From molecules to materials: Pre-training large generalizable models for atomic property prediction, 2024.
- Smith, J. S., Zubatyuk, R., Nebgen, B., Lubbers, N., Barros, K., Roitberg, A. E., Isayev, O., and Tretiak, S. The ani-1ccx and ani-1x data sets, coupled-cluster and density functional theory properties for molecules. *Scientific data*, 7(1):1–10, 2020.
- Tran, R., Lan, J., Shuaibi, M., Wood, B. M., Goyal, S., Das, A., Heras-Domingo, J., Kolluru, A., Rizvi, A., Shoghi, N., Sriram, A., Therrien, F., Abed, J., Voznyy, O., Sargent, E. H., Ulissi, Z., and Zitnick, C. L. The open catalyst 2022 (oc22) dataset and challenges for oxide electrocatalysts. *ACS Catalysis*, 13(5):3066–3084, February 2023. ISSN 2155-5435. doi: 10.1021/acscatal.2c05426. URL <http://dx.doi.org/10.1021/acscatal.2c05426>.
- Wang, Y., Sun, Y., Liu, Z., Sarma, S. E., Bronstein, M. M., and Solomon, J. M. Dynamic graph cnn for learning on point clouds, 2019.
- Zaidi, S., Schaarschmidt, M., Martens, J., Kim, H., Teh, Y. W., Sanchez-Gonzalez, A., Battaglia, P., Pascanu, R., and Godwin, J. Pre-training via denoising for molecular property prediction, 2022.

## A. Canonicalization

### A.1. Stochastic Frame Averaging

**Frame Averaging** We recall the idea of Frame Averaging introduced by [Puny et al. \(2021\)](#), in which  $\mathcal{X}$  and  $\mathcal{Y}$  denote normed linear space with respective representations  $\rho_1$  and  $\rho_2$  of a group  $G$ . In our case, the group of interest is  $E(3)$ . A *frame* is defined as a function  $\mathcal{F} : \mathcal{X} \rightarrow 2^G$  taking values in a non-empty subset of the group  $G$  such that it is  $G$ -equivariant and bounded. Under such conditions, and for every  $\Phi : \mathcal{X} \rightarrow \mathcal{Y}$ , the function  $\langle \Phi \rangle_{\mathcal{F}} : \mathcal{X} \rightarrow \mathcal{Y}$ , called *average over the frame*  $\mathcal{F}$ , and defined as

$$\langle \Phi \rangle_{\mathcal{F}} : x \mapsto \frac{1}{|\mathcal{F}(x)|} \sum_{g \in \mathcal{F}(x)} \rho_2(g) \Phi(\rho_1(g)^{-1}x), \quad (1)$$

is  $G$ -equivariant. This allows to create an arbitrary neural network, and guarantee the symmetry by averaging the outputs over a well-chosen frame.

**Choosing the frame.** As in [Duval et al. \(2023\)](#), the neural network takes as input  $X$  the atoms position,  $Z$  is their atomic numbers, and has outputs in  $\mathcal{Y}$ , where  $\mathcal{Y} = \mathbb{R}^{n \times 3}$  in the case of force predictions, and  $\mathcal{Y} = \mathbb{R}$  in the case of energy prediction. The group  $E(3)$  only acts on  $X$ , and not  $Z$ . A Principal Component Analysis (PCA) on the atomic structure allows to decompose the covariance matrix of the points cloud  $\Sigma = U^T \Lambda U$  derived from the centroid of the positions  $t = \frac{1}{n} X^T \mathbf{1}$ , with  $\Lambda$  the diagonal matrix containing the three eigenvalues  $\lambda_1 > \lambda_2 > \lambda_3$  (assumed distinct because we consider non-planar structures). The frame is taken as

$$\mathcal{F}(X) = \{(U, t) \mid U = [\pm u_1, \pm u_2, \pm u_3]\}, \quad (2)$$

which is a subset of  $E(3)$ . The authors prove that the frame  $\mathcal{F}$  defined as such is  $G$ -equivariant and bounded.

**Stochastic Frame Averaging.** This process requires to average the predictions of the neural network over  $|\mathcal{F}(X)| = 2^3 = 8$  elements of the frame. In order to make the computations faster, [Duval et al. \(2023\)](#) sample only one element from the frame instead of performing the average. Although Stochastic Frame-Averaging (SFA) does not have theoretical guarantees, it has been experimentally shown to learn almost perfect equivariance.

### A.2. SFA+SignNet

Initially proposed to help spectral graph representation learning, SignNet ([Lim et al., 2023b](#)) is a network which outputs are invariant to sign flips. The authors state that a continuous function  $\eta : \mathbb{R}^n \rightarrow \mathbb{R}^d$  is *sign-invariant* if and only if  $\eta(x) = \kappa(x) + \kappa(-x)$  for some (freely chosen) continuous function  $\kappa : \mathbb{R}^n \rightarrow \mathbb{R}^d$ . SignNet :  $\mathbb{R}^{n \times k} \rightarrow \mathbb{R}^{n \times k}$  is then defined as:

$$\text{SignNet}(x_1, \dots, x_k) = \mu([\kappa(x_i) + \kappa(-x_i)]_{i=1}^k), \quad (3)$$

where  $\mu$  and  $\kappa$  are neural networks chosen freely.

We propose to apply such a network on the sampled element of the frame  $U$  and parametrize  $\mu$  and  $\kappa$  either with MLPs or with VN-PointNets. In order to constrain the output, we further orthonormalize the output with a Gram-Schmidt process:

$$U' = \text{Gram-Schmidt}(\text{SignNet}(U)). \quad (4)$$

When parametrizing SignNet with MLPs, since we apply non-linearities on the orthogonal matrix  $U$ , there is no theoretical guarantee for the whole process to be  $E(3)$ -equivariant a priori. This is coherent with empirical observations when using this method, although training  $\mu$  and  $\kappa$  helps better enforce the equivariance.

When parametrizing SignNet with VN-PointNets, the whole network is made exactly  $E(3)$ -equivariant. As explained by [Lim et al. \(2023a\)](#) (section 2.2), the matrix  $U$  is orthogonal and unique up to sign changes, while the SignNet function is both sign invariant by design and  $O(3)$ -equivariant thanks to the use of VN-PointNets.

### A.3. Vector Neurons Network

VNNs are a class of  $SO(3)$ -equivariant models, where usual neurons are replaced with so-called Vector Neurons: for a given layer, non-linearities output a matrix of size  $h \times 3$  instead of a vector of length  $h$ .

Using this framework, [Deng et al. \(2021\)](#) re-implement classic operations such as linear layers, non-linearities, pooling operations, and normalization layers. They also prove that those layers are all  $SO(3)$ -equivariants, which allows to re-implement classical networks into their VN variant. In particular, they re-implement the VN variants of two well-known networks from the point clouds literature: PointNet ([Qi et al., 2017](#)) and DGCNN ([Wang et al., 2019](#)), and test them on classification, segmentation, and reconstruction tasks. They show that accuracy increases compared to the classic implementations and that their equivariance property is indeed (almost) perfectly enforced.

To obtain an  $O(3)$  (and then  $E(3)$ ) equivariance, the output of the VNN has to be further orthonormalized with a Gram-Schmidt process to canonicalize the representation in  $O(3)$ , as described by [Kaba et al. \(2023\)](#).

The following Vector Neurons Networks (VNNs) are used:

- VN-Pointnet with a varying number of VNLinearLeakyReLU layers (between 1 and 3), with the implementation of [Deng et al. \(2021\)](#).
- VN-DGCNN, with the implementation is the one of [Deng et al. \(2021\)](#).

To summarize, we use VNNs to learn the transformation  $U$  from the positions  $X$ :

$$\begin{aligned} \text{VNN} : \mathbb{R}^{n \times 3} &\rightarrow \mathbb{R}^{3 \times 3} \\ X &\mapsto U. \end{aligned}$$

$U$  is then orthonormalized with a Gram-Schmidt process.

#### A.4. Experimental comparisons

OC20 IS2RE: Tables 5 and 6

OC20 S2EF: Tables 7 and 8

QM9: Table 9

In all OC20 experiments of this section, for a fair assessment, SFA is used in 3D mode, i.e. without the computational trick to force the  $z$  axis to remain fixed during canonicalization, which is specific to OC20. The same goes for the methods derived from SFA. As a consequence, the reported performances are lower than reported in other sections.

Canonicalization	Cano. trainable parameters	2D Rotation ↓ Invariance	3D Rotation ↓ Invariance	Reflection ↓ Invariance
SFA	0	$1.29 \cdot 10^{-2}$	$1.32 \cdot 10^{-2}$	$1.30 \cdot 10^{-2}$
Untrained SFA+MLP-SignNet	0	$1.01 \cdot 10^{-1}$	$1.00 \cdot 10^{-1}$	$9.71 \cdot 10^{-2}$
Trained SFA+MLP-SignNet	454	$4.21 \cdot 10^{-2}$	$7.74 \cdot 10^{-2}$	$4.00 \cdot 10^{-2}$
Untrained SFA+VN-SignNet	0	$6.89 \cdot 10^{-3}$	$7.58 \cdot 10^{-3}$	$7.37 \cdot 10^{-3}$
Trained SFA+VN-SignNet	2,620	$2.45 \cdot 10^{-2}$	$2.66 \cdot 10^{-2}$	$2.43 \cdot 10^{-2}$
Untrained VN-Pointnet (2 hid.)	0	$4.61 \cdot 10^{-3}$	$4.62 \cdot 10^{-3}$	$4.62 \cdot 10^{-3}$
Trained VN-Pointnet (2 hid.)	1,310	<b><math>3.63 \cdot 10^{-3}</math></b>	<b><math>3.72 \cdot 10^{-3}</math></b>	<b><math>3.80 \cdot 10^{-3}</math></b>
Untrained VN-Pointnet (1 hid.)	0	$4.28 \cdot 10^{-3}$	$4.28 \cdot 10^{-3}$	$4.29 \cdot 10^{-3}$
Untrained VN-Pointnet (0 hid.)	0	$2.76 \cdot 10^{-2}$	$2.76 \cdot 10^{-2}$	$2.79 \cdot 10^{-2}$
Trained VN-Pointnet (0 hid.)	24	$1.86 \cdot 10^{-2}$	$2.31 \cdot 10^{-2}$	$2.36 \cdot 10^{-2}$
Untrained VN-DGCNN	0	$3.03 \cdot 10^{-2}$	$3.08 \cdot 10^{-2}$	$3.11 \cdot 10^{-2}$
Trained VN-DGCNN	663,804	$9.89 \cdot 10^{-3}$	$2.49 \cdot 10^{-2}$	$9.10 \cdot 10^{-3}$

Table 5. Invariance comparison of canonicalization methods on OC20 IS2RE dataset. The FAENet backbone for this task and dataset has 4,147,731 parameters (5 interaction blocks). We measure the rotation invariance and reflection invariance property as the difference in prediction between every samples D1 (of the ID val split) and D2 defined as a  $SO(3)$  transformation of D1, in eV.

## Improving Molecular Modeling with Geometric GNNs: an Empirical Study

Canonicalization	ID		OOD-CAT		OOD-ADS		OOD-BOTH	
	EwT (%) $\uparrow$	MAE (meV) $\downarrow$						
SFA	4.40	566	4.12	563	2.56	652	2.77	594
Untrained SFA+MLP-SignNet	4.48	<b>554</b>	4.46	552	2.75	<b>637</b>	2.88	<b>576</b>
Trained SFA+MLP-SignNet	4.46	<b>554</b>	4.51	<b>551</b>	2.67	642	2.78	586
Untrained SFA+VN-SignNet	<b>4.69</b>	563	4.60	558	2.62	651	2.59	595
Trained SFA+VN-SignNet	4.25	572	4.27	568	<b>2.92</b>	658	<b>2.97</b>	596
Untrained VN-Pointnet (2 hid.)	4.09	567	<b>4.66</b>	565	2.60	673	2.85	615
Trained VN-Pointnet (2 hid.)	4.12	568	4.33	563	2.77	658	2.75	604
Untrained VN-Pointnet (1 hid.)	4.37	565	4.20	561	2.64	666	2.73	614
Untrained VN-Pointnet (0 hid.)	4.01	581	3.92	571	2.75	660	2.64	615
Trained VN-Pointnet (0 hid.)	4.14	567	4.36	563	2.56	675	2.88	614
Untrained VN-DGCNN	4.31	567	4.14	562	2.58	660	2.72	610
Trained VN-DGCNN	4.42	560	4.40	556	2.78	656	2.81	601

Table 6. Performance comparison of canonicalization methods on OC20 IS2RE dataset. All models were trained for 12 epochs using Duval et al. (2023) config.

Canonicalization	Cano. trainable parameters	Energy invariance		Forces equivariance	
		3D Rotation $\downarrow$	Reflection $\downarrow$	3D Rotation $\downarrow$	Reflection $\downarrow$
SFA	0	$1.88 \cdot 10^{-2}$	$1.88 \cdot 10^{-2}$	$7.17 \cdot 10^{-2}$	$8.34 \cdot 10^{-3}$
Untrained SFA+MLP-SignNet	0	$7.81 \cdot 10^{-2}$	$7.61 \cdot 10^{-2}$	$7.44 \cdot 10^{-2}$	$2.04 \cdot 10^{-2}$
Trained SFA+MLP-SignNet	454	$6.57 \cdot 10^{-2}$	$3.57 \cdot 10^{-2}$	$7.35 \cdot 10^{-2}$	$1.17 \cdot 10^{-2}$
Untrained SFA+VN-SignNet	0	$2.07 \cdot 10^{-2}$	$2.04 \cdot 10^{-2}$	$6.86 \cdot 10^{-2}$	$9.42 \cdot 10^{-3}$
Trained SFA+VN-SignNet	2,620	$1.92 \cdot 10^{-2}$	$1.89 \cdot 10^{-2}$	$6.55 \cdot 10^{-2}$	$8.72 \cdot 10^{-3}$
Untrained VN-Pointnet (2 hid.)	0	$1.80 \cdot 10^{-2}$	$1.80 \cdot 10^{-2}$	$6.92 \cdot 10^{-2}$	$8.78 \cdot 10^{-3}$
Trained VN-Pointnet (2 hid.)	1,310	$1.67 \cdot 10^{-2}$	$1.67 \cdot 10^{-2}$	$6.89 \cdot 10^{-2}$	$8.77 \cdot 10^{-3}$
Untrained VN-Pointnet (0 hid.)	0	$3.50 \cdot 10^{-2}$	$3.49 \cdot 10^{-2}$	$6.96 \cdot 10^{-2}$	$1.08 \cdot 10^{-2}$
Trained VN-Pointnet (0 hid.)	24	$3.31 \cdot 10^{-2}$	$3.34 \cdot 10^{-2}$	$7.00 \cdot 10^{-2}$	$1.05 \cdot 10^{-2}$
Untrained VN-DGCNN	0	<b><math>1.50 \cdot 10^{-2}</math></b>	<b><math>1.50 \cdot 10^{-2}</math></b>	<b><math>6.83 \cdot 10^{-2}</math></b>	<b><math>3.58 \cdot 10^{-3}</math></b>
Trained VN-DGCNN	663,804	$2.02 \cdot 10^{-2}$	$1.50 \cdot 10^{-2}$	$6.91 \cdot 10^{-2}$	$8.09 \cdot 10^{-3}$

Table 7. Equivariance comparison of canonicalization methods on OC20 S2EF dataset. The FAENet backbone for this task and dataset has 5,675,410 parameters (7 interaction blocks). We measure the energy rotation invariance, energy reflection invariance, force rotation equivariance, and force reflection equivariance properties as the difference in prediction between every sample D1 (of the ID val split) and D2 defined as a SO(3) transformation of D1, in eV.

## Improving Molecular Modeling with Geometric GNNs: an Empirical Study

Canonicalization	Energy MAE (mEV) ↓				Force MAE (mEV) ↓			
	ID	OOD Cat	OOD Ads	OOD Both	ID	OOD Cat	OOD Ads	OOD Both
SFA	424	445	579	680	55.6	55.2	63.2	74.6
Untrained SFA+MLP-SignNet	<b>420</b>	<b>444</b>	<b>515</b>	<b>631</b>	<b>54.0</b>	<b>53.8</b>	<b>61.4</b>	<b>72.4</b>
Trained SFA+MLP-SignNet	422	446	558	666	54.2	53.9	62.7	73.8
Untrained SFA+VN-SignNet	439	458	565	673	56.5	56.0	65.3	76.7
Trained SFA+VN-SignNet	442	464	590	701	58.0	57.5	65.2	76.9
Untrained VN-Pointnet (2 hid.)	435	455	596	697	56.0	55.6	66.9	77.5
Trained VN-Pointnet (2 hid.)	435	453	585	696	56.1	55.8	64.2	75.6
Untrained VN-Pointnet (0 hid.)	440	459	597	705	56.0	55.6	64.7	75.8
Trained VN-Pointnet (0 hid.)	440	459	572	671	55.8	55.4	63.7	74.9
Untrained VN-DGCNN	456	474	593	763	55.7	55.5	65.8	76.9
Trained VN-DGCNN	432	453	662	762	55.5	55.2	71.2	80.7

Table 8. Performance comparison of canonicalization methods on OC20 S2EF dataset. All models were trained for 12 epochs using Duval et al. (2023) config.

Canonicalization	Cano. trainable parameters	MAE (meV) ↓		Energy invariance (eV)	
		ID	Test	3D Rotation ↓	Reflection ↓
SFA	0	<b>9.20</b>	<b>9.06</b>	$1.65 \cdot 10^{-3}$	$1.76 \cdot 10^{-3}$
Untrained SFA+MLP-SignNet	0	11.3	11.2	$2.12 \cdot 10^{-3}$	$2.20 \cdot 10^{-3}$
Trained SFA+MLP-SignNet	454	10.5	10.7	$1.60 \cdot 10^{-3}$	$1.66 \cdot 10^{-3}$
Untrained SFA+VN-SignNet	0	9.41	9.40	$1.28 \cdot 10^{-3}$	$1.37 \cdot 10^{-3}$
Trained SFA+VN-SignNet	2,620	10.1	10.2	$1.33 \cdot 10^{-3}$	$1.40 \cdot 10^{-3}$
Untrained VN-Pointnet (2 hid.)	0	10.4	10.3	<b><math>1.19 \cdot 10^{-3}</math></b>	$1.30 \cdot 10^{-3}$
Trained VN-Pointnet (2 hid.)	1,310	10.1	9.85	$1.30 \cdot 10^{-3}$	$1.44 \cdot 10^{-3}$
Untrained VN-Pointnet (0 hid.)	0	9.51	9.49	$1.21 \cdot 10^{-3}$	<b><math>1.24 \cdot 10^{-3}</math></b>
Trained VN-Pointnet (0 hid.)	24	11.4	11.5	$1.64 \cdot 10^{-3}$	$1.74 \cdot 10^{-3}$
Untrained VN-DGCNN	0	9.92	9.94	$1.32 \cdot 10^{-3}$	$1.46 \cdot 10^{-3}$
Trained VN-DGCNN	663,804	9.34	9.25	$1.79 \cdot 10^{-3}$	$1.79 \cdot 10^{-3}$

Table 9. Equivariance and performance comparison of canonicalization methods on QM9 dataset for the target property  $U_0$  (internal energy at 0 Kelvin). The FAENet backbone for this task has 6,495,127 parameters (5 interaction blocks). We measure the energy rotation invariance as the difference in prediction between every samples D1 (of the ID val split) and D2 defined as a SO(3) transformation of D1, in eV. All models were trained for 300 epochs using Duval et al. (2023) config.

### A.5. Relaxations from S2EF model for IS2RE

The models used to run the experiments with the relaxation methods were trained on the 2M train split of the S2EF dataset from OC20. This dataset has been shown to converge to similar performances as the complete dataset, which is way larger and takes too long to train on (Gasteiger et al., 2022). We report in Table 10 the performances of these models, which might help interpret some of the results for the relaxation.

Model	EwT ↓	Force MAE ↓	Forces cos ↑
FAENet with SFA	10.7	0.044	0.32
FAENet with Untrained PointNet	10.5	0.0043	0.33
FAENet without SFA	10.0	0.042	0.34
SchNet Base	5.1	0.061	0.07

Table 10. Performance comparison of models on OC20 S2EF dataset on the VAL-ID split. The energy within threshold, Force MAE, and cos similarity are reported for these S2EF models that are then used for relaxations. Note that this method yields way longer training and inference times when compared to direct IS2RE as reported.

## B. Graph creation study

### B.1. Cutoff

The cutoff defines the distance within which a link between two atoms is created. All atoms that are at a distance smaller than this cutoff will be linked. However, in order to avoid cluttering the created graphs, most methods impose a maximum number of neighbors for every atom. This parameter is usually taken around 40 neighbors.

Model	ID		OOD-ADS		OOD-CAT		OOD-BOTH	
	EwT (%) $\uparrow$	MAE (eV) $\downarrow$						
Cutoff 30 - Max neighbours 40	2.65	0.697	1.45	0.906	2.86	0.691	1.53	0.846
Cutoff 20 - Max. neighbours 40	3.08	0.673	1.85	0.808	2.86	0.669	1.86	0.757
Cutoff 20 - Max. neighbours 10	2.25	0.768	1.51	0.988	2.52	0.754	1.38	0.928
Cutoff 10 - Max. neighbours 50	4.17	0.553	2.81	0.640	4.12	0.551	3.02	0.585
Cutoff 10 - Max. neighbours 40	4.29	0.555	2.95	0.631	4.33	0.553	2.71	0.587
Cutoff 10 - Max. neighbours 30	4.43	0.551	2.65	0.655	4.51	0.552	2.51	0.611
Cutoff 10 - Max. neighbours 20	4.38	0.551	2.46	0.676	4.45	0.551	2.55	0.621
Cutoff 10 - Max. neighbours 10	4.49	0.553	2.84	0.627	4.34	0.549	3.01	0.582
Cutoff 6 - Max. neighbours 40	4.31	0.553	3.00	0.626	4.39	0.554	2.81	0.577
Cutoff 1 - Max. neighbours 40	1.35	1.069	1.32	1.112	1.33	1.051	1.37	1.018

Table 11. Impact of the cutoff on the performances of FAENet on the OC20 IS2RE task. Full table on all validation splits.

### B.2. Ewald-based Long-Range Message Passing

The main idea behind Ewald summation used in section 3.2 is to decompose the electrostatic interaction potential with a given charge into a short-range interaction and a long-range interaction term. The short-range contribution can be computed with real spatial features and the long-range contribution is computed using a Fourier transform. This principle is illustrated in Figure 3. This allows for computational methods in electrostatics to converge faster and with higher accuracy because the long-range interaction becomes more tractable.

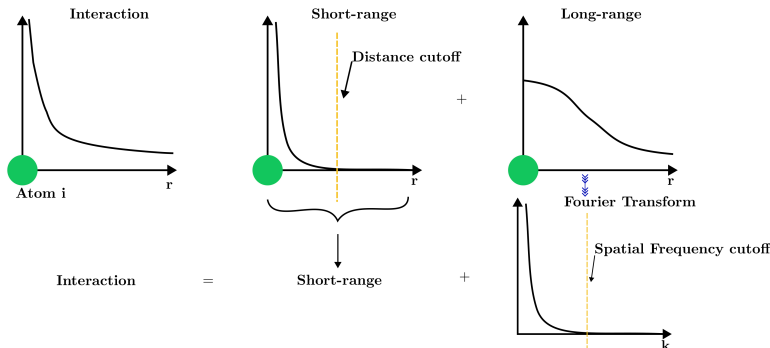


Figure 3. Ewald Summation interactions. The interaction term (left) is the result of the short-range interaction (middle) and the long-term interaction (right) which are both computed using cutoffs on respectively the real and the Fourier space. Adapted from (Kosmala et al., 2023)

In the case of GNNs, the short-range interaction is already computed by the currently implemented interaction blocks using a distance cutoff between the atoms, which omits the negligible parts of this interaction for further atoms. However, the heavy-tail of long-range interactions is then reported to a new term in real space, which doesn't diverge anymore for closer atoms. It can then be computed using the same cutoff idea but in the Fourier space where a *spatial frequency cutoff* is used to make it tractable as introduced in Kosmala et al. (2023).

**Periodic case.** In the case where there exists a spatial periodic tiling of materials (OC20 for example), it is possible to define the set of periodic cells localization  $\Lambda = \{\lambda_1 \mathbf{v}_1, \lambda_2 \mathbf{v}_2, \lambda_3 \mathbf{v}_3 \mid (\lambda_1, \lambda_2, \lambda_3) \in \mathbb{Z}^3\}$ , where  $\mathbf{v}_1, \mathbf{v}_2, \mathbf{v}_3$  define the periodic cell lattice, similarly to the periodic interval in the 1D case. In the real space, the long-range interaction component would be written as a sum over all of the elements on the infinite tiling, which can be decomposed as a Fourier series

expansion using the reciprocal lattice  $\Lambda'$ . This reciprocal lattice would be similar to the  $2\pi$  in the 1D case of the Fourier transform. It is the periodic space of all the wavevectors of the Fourier series. This results in the proposed expansion for Ewald message passing:

$$M^{lr}(x_i) = \sum_{\mathbf{k} \in \Lambda'} \exp(i\mathbf{k}^T x_i) \cdot \sum_{j \in S} h_j \exp(-i\mathbf{k}^T x_j) \cdot \hat{\Phi}^{lr}(\|\mathbf{k}\|), \quad (5)$$

where  $M^{lr}(x_i)$  corresponds to the long-range message computed at node  $i$  from all of the nodes in the system  $S$ , and  $\hat{\Phi}^{lr}$  is a learned Fourier coefficient of a radial basis function representing the interaction. The cutoff in the Fourier basis  $c_k$  is then set to make the sum finite over the set  $\{k \in \Lambda', \|\mathbf{k}\| \leq c_k\}$ . Since the number of wavevectors used for the computation is finite,  $\hat{\Phi}(\|\mathbf{k}\|)$  is learned for every  $\mathbf{k}$ . Since Ewald summation applies to periodic structures, the authors of Ewald message passing [Kosmala et al. \(2023\)](#) propose tricks to deal with the aperiodic case by assuming an infinite tiling.

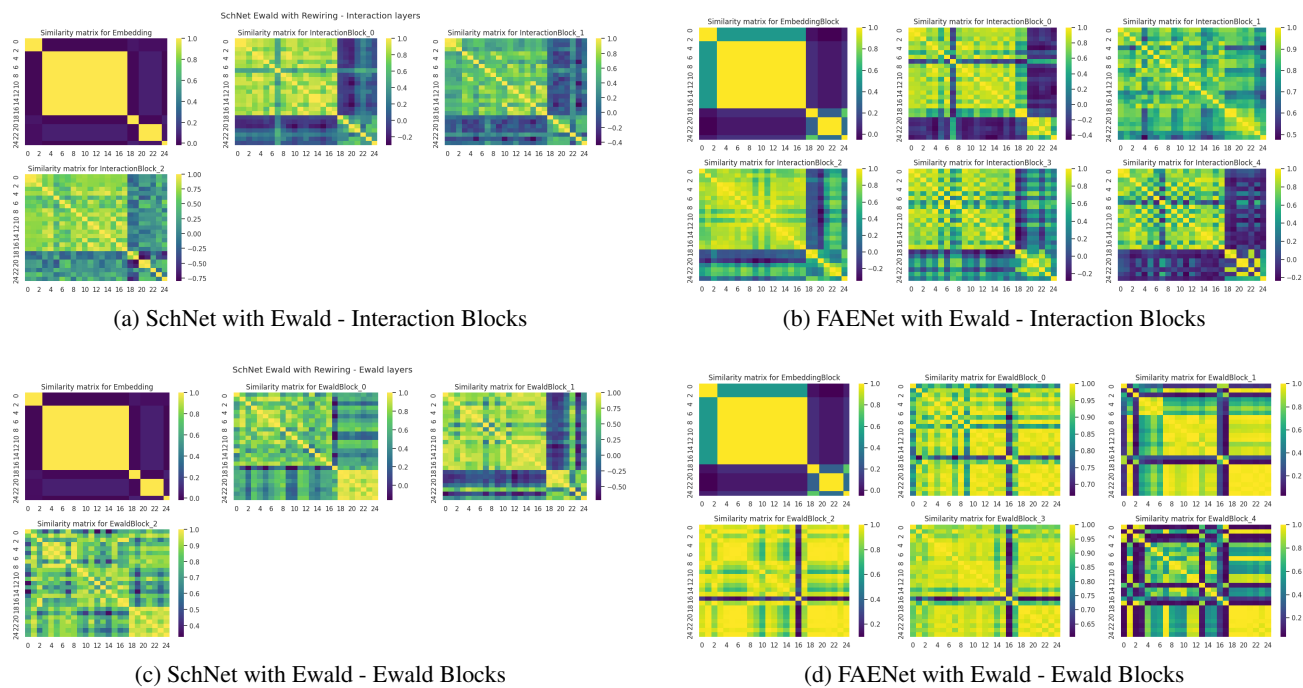


Figure 4. Similarity matrix of the embeddings of the atoms of a system for different interaction blocks on FAENet and SchNet with Ewald message passing on the models. The visualized layers here are the standard interaction blocks in the first row and the Ewald interaction blocks in the second row. The two outputs are summed to get the final representation for Ewald shown in Figure 1.

## Improving Molecular Modeling with Geometric GNNs: an Empirical Study

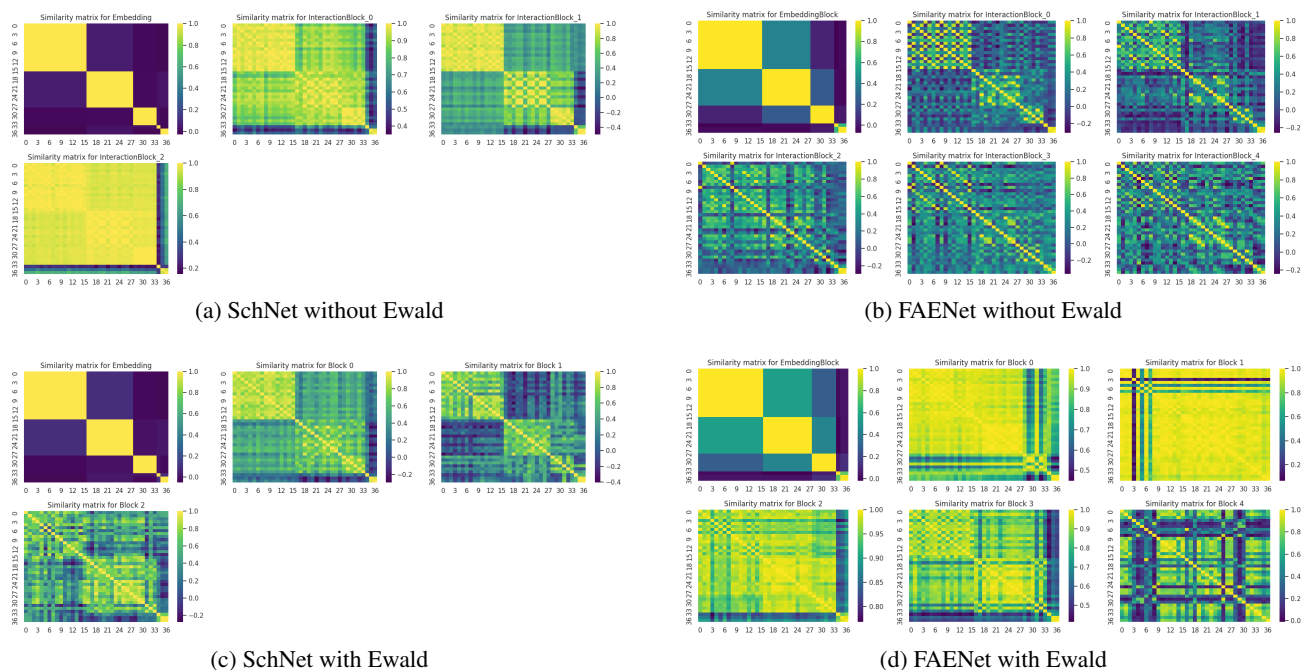


Figure 5. Same plots as Figure 1 but with a second randomly picked system from the OC20 train split.

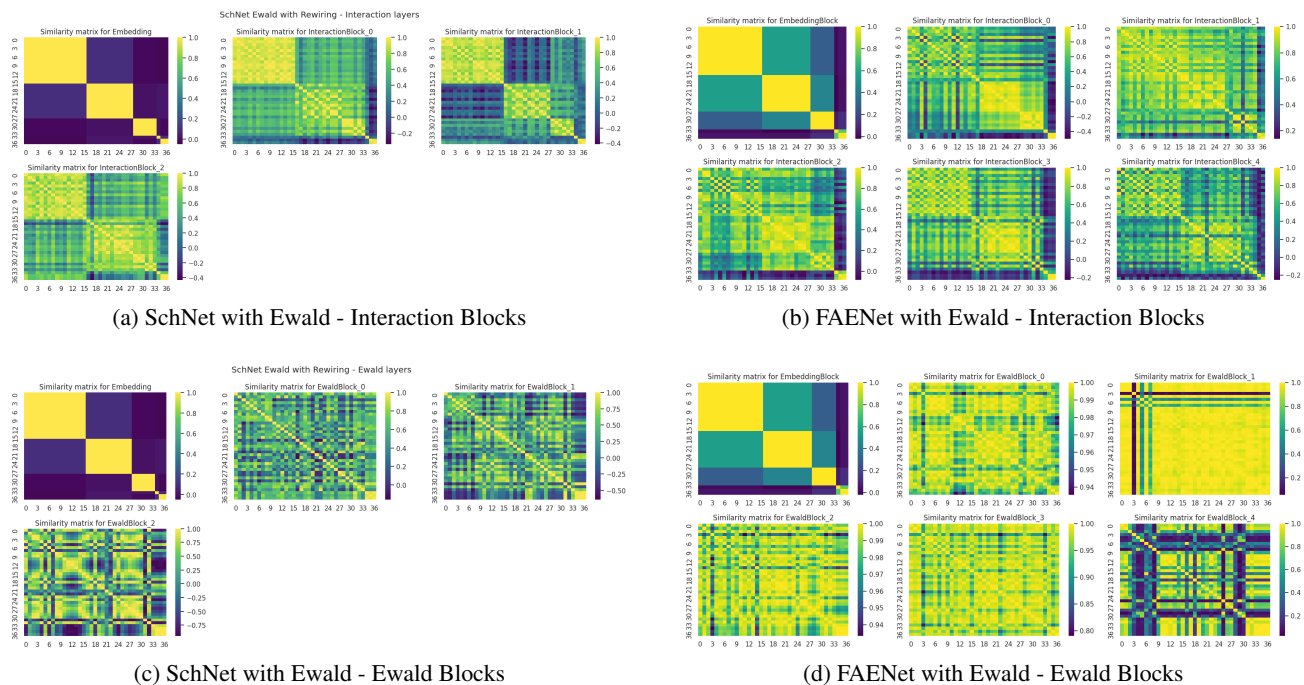


Figure 6. Same plots as Figure 4 but with a second randomly picked system from the OC20 train split.

## Improving Molecular Modeling with Geometric GNNs: an Empirical Study

Model	ID		OOD-ADS		OOD-CAT		OOD-BOTH	
	EwT (%) $\uparrow$	MAE (eV) $\downarrow$						
FAENet (Graph Rewiring)	4.05	0.551	2.65	0.650	4.29	0.550	2.76	0.601
FAENet (Graph Rewiring) + Ewald	4.12	0.562	2.68	0.648	4.14	0.563	2.83	0.597
FAENet (No Graph Rewiring)	4.54	0.544	2.59	0.657	4.66	0.539	2.65	0.601
FAENet (No Graph Rewiring) + Ewald	4.11	0.556	2.75	0.626	4.13	0.553	2.85	0.569
SchNet (Graph Rewiring)	3.18	0.641	2.53	0.720	3.00	0.638	2.59	0.642
SchNet (Graph Rewiring) + Ewald	3.54	0.604	2.53	0.665	3.53	0.599	2.67	0.608
SchNet (No Graph Rewiring)	2.93	0.654	2.22	0.700	3.04	0.646	2.54	0.656
SchNet (No Graph Rewiring) + Ewald	3.48	0.597	2.76	0.647	3.56	0.599	2.73	0.612

Table 12. Energy prediction errors with and without Ewald Message Passing. Graph Rewiring refers to removing the subsurface atoms from the system (Duval et al., 2022). In this table, FAENet is taken with 5 interaction layers (top config), while SchNet uses 3 interaction layers.

Model	MAE (meV) $\downarrow$	MSE ((meV) <sup>2</sup> ) $\downarrow$
FAENet	8.44	0.600
FAENet + Ewald	8.34	0.574
SchNet	16.0	1.18
SchNet + Ewald	11.5	0.73

Table 13. Energy prediction errors with and without Ewald Message Passing on the test split of the QM9 dataset for the target property  $U_0$  (Internal energy at 0K).

## C. Noisy Nodes

### C.1. Experimental setup

Runs are done on a single Nvidia Quadro RTX 8000 GPU with 48 GB memory or, if indicated, on a single Nvidia A100 GPU with 80 GB memory.

### C.2. Noisy Nodes implementation

In practice, we perturb the input node positions of the graph  $G$  with a noise  $\sigma$  and train the model with two loss terms, a Noisy Nodes loss term and the primary loss (associated with the main task) term

$$\mathcal{L} = \lambda \cdot \mathcal{L}_{NNodes}(\hat{G}', V') + \mathcal{L}_{Primary}(\hat{G}', V'), \quad (6)$$

where  $\lambda$  is the weight we assign to the auxiliary denoising task,  $\hat{G}' = \tilde{\Phi}(\tilde{G})$  is the output of the model  $\tilde{\Phi}$ ,  $\tilde{G}$  is the noised graph, and  $V'$  can either be the target nodes features (e.g. atom positions at equilibrium, that is the IS2RS task) or the initial nodes positions (see next subsection on denoising pre-training).

For the input, we first interpolate between initial structure and relaxed structure and then add Gaussian noise, that is for each node  $i$ , the input positions of the input "Noisy Nodes graph"  $\tilde{x}^i$  are defined as

$$\tilde{x}^i = \begin{cases} \gamma(x_{rel}^i - x_{init}^i) + Z^i & \text{with probability } 0.5 \\ x_{init}^i & \text{with probability } 0.5, \end{cases} \quad (7)$$

with random interpolation factor  $\gamma \sim U[0, 1]$  independent between graphs and iid Gaussian noises  $Z^i \sim \mathcal{N}(0, \sigma)$  with  $\sigma = 0.3$ . The Noisy Nodes target is  $\Delta_{pos}^i = x_{rel}^i - \tilde{x}^i$  and therefore the auxiliary loss term is  $\|\Delta_{pos}^i - \Phi(\tilde{x}^i)\|_1$  for the model  $\Phi$ . Our total loss is the sum of the energy MAE loss and the auxiliary loss weighted by a number  $\lambda$ , as in Equation 6. Both the primary loss and Noisy Nodes Loss (before multiplication by  $\lambda$ ) typically have the same value between 1 and 2.5.

For the IS2RE training, we add a position decoding head to the preexisting energy prediction head. The position decoding head, as with the force prediction head introduced in (Duval et al., 2023), is a 2-layer MLP with Batchnorm.

### C.3. Related work

Since Noisy Nodes performs denoising as an auxiliary task during training, the representation learning benefits of denoising are limited to the downstream dataset on which the model is trained. Zaidi et al. (2022) propose to rather perform denoising

as a pre-training objective on a large, unlabelled dataset of atomic structures.

Shoghi et al. (2024) introduce Joint Multi-domain Pre-training (JMP), a supervised pre-training strategy that simultaneously trains on various datasets from different chemical domains (OC20 (Chanussot et al., 2020), OC22 (Tran et al., 2023), ANI-1x (Smith et al., 2020), and Transition-1x (Schreiner et al., 2022)), treating each dataset as a unique pre-training task within a multi-task framework.

#### C.4. Training hyperparameters

The most obvious changes to the training hyperparameters that should theoretically allow to leverage the denoising auxiliary task are to increase the depth of the network and the number of epochs. First, we observe that we reach convergence on the validation set for the energy MAE more slowly when using the auxiliary task because of a more complex loss to minimize and a higher number of model weights (due to the supplementary interaction blocks). Hence, unless otherwise stated, the number of epochs is 50 in the IS2RE with IS2RS auxiliary task experiments.

(Liao & Smidt, 2023) use a linearly decaying weight from 15 to 1 for the auxiliary IS2RS loss to encourage the model to learn more from the auxiliary task in the beginning but focus on the primary task at the end of training. We also tested a constant auxiliary weight of 1, a weight decaying from 30, and cosine annealing with a linear warmup scheduler, but this yielded worse or equivalent results. Thus, unless otherwise stated, we always use as an auxiliary weight scheduler the one of Equiformer in the following IS2RE with IS2RS auxiliary task experiments.

Since we always use the MAE as energy loss for the IS2RE main task, it proves essential to use the MAE loss for the auxiliary position loss to leverage the benefits of Noisy Nodes. Indeed, our experiments using the MSE position loss led to a collapse of the node embeddings at the last interaction layers, that could be observed by plotting the MAD throughout the interaction layers.

#### C.5. Results

##### C.5.1. COMPARING DEPTH FOR CLASSICAL FAENET

In the results of Table 14, the number of warmup steps is 6000 for about 180k steps. The batch size is 128, hence the lower throughput than the one with the same configs of (Duval et al., 2023). In these runs, the hyperparameters are the top configs of (Duval et al., 2023) except for slight differences: the number of hidden channels in the embedding blocks is a bit lower. Also, contrary to the top configs of (Duval et al., 2023), we train for 50 epochs (instead of 12) with no early stopping to be in a comparable setup to the IS2RE with IS2RS auxiliary task models.

Interaction blocks	Parameters (millions)	Time		Energy MAE (meV) ↓					EwT (%) ↑				
		Train ↓	Infer. ↑	ID	OOD Ads	OOD Cat	OOD Both	Average	ID	OOD Ads	OOD Cat	OOD Both	Average
5	5.9	19min	786	556	685	552	636	607	4.41	2.26	4.51	2.47	3.41
8	9.2	25min	676	554	643	558	596	<b>588</b>	4.31	2.66	4.40	2.75	<u>3.53</u>
10	11.4	29min	621	552	649	554	603	<u>590</u>	4.56	2.77	4.20	2.72	<b>3.56</b>
12	13.7	34min	527	551	661	556	609	594	4.01	2.57	4.21	2.53	3.33
14	15.9	37min	498	621	749	608	693	668	3.42	2.06	3.27	2.31	2.77
16	18.2	40min	457	590	704	592	647	633	4.05	2.51	3.90	2.53	3.25

Table 14. Comparison varying the number of interaction blocks for FAENet without auxiliary task with the top configs of (Duval et al., 2023) except for slight differences. Scalability is measured with training time for one epoch (Train, in minutes) and inference throughput (Infer., number of samples processed in a second). The best score is in bold and the second-best score is underlined. Performances are slightly worse than the best performances presented in (Duval et al., 2023) because of different hyperparameters, but the main conclusion is that the performances worsen when we add interaction layers after 12.

##### C.5.2. COMPARING DEPTH FOR FAENET WITH NOISY NODES IS2RS AUXILIARY TASK

In Table 15, we observe a clear positive correlation between the depth of the model and its performances in terms of energy MAE and EwT. The gain in performance is very clear between 5 and 16 interaction layers, then increases much more slowly up to 28 layers.

## Improving Molecular Modeling with Geometric GNNs: an Empirical Study

Interaction blocks	Parameters (millions)	Time		Energy MAE (meV) ↓					EwT (%) ↑				
		Train ↓	Infer. ↑	ID	OOD Ads	OOD Cat	OOD Both	Average	ID	OOD Ads	OOD Cat	OOD Both	Average
5	4.2	17min	724	523	592	525	545	546	4.59	2.92	4.40	3.15	3.76
8	6.6	22min	679	518	600	526	561	551	5.13	2.88	5.21	2.74	3.99
10	8.1	27min	584	513	606	521	561	550	5.17	2.82	5.03	2.81	3.96
12 (A100)	9.7	30min	504	517	589	523	546	544	5.10	3.17	4.92	3.04	4.06
14	11.2	33min	525	507	580	519	541	537	5.20	3.13	5.21	3.25	4.20
16	12.8	35min	465	505	566	516	527	<u>529</u>	5.17	3.63	5.00	3.69	4.37
18	14.3	38min	446	508	596	518	554	544	5.31	3.22	5.58	2.97	4.27
20	15.9	42min	423	508	593	513	553	542	5.39	3.16	5.18	2.88	4.15
22	17.4	45min	401	507	569	515	528	530	5.24	3.26	5.06	3.32	4.22
24	19.0	48min	375	500	574	510	534	<u>529</u>	5.70	3.43	5.43	3.31	<b>4.47</b>
26	20.6	50min	335	504	562	512	521	<b>525</b>	5.15	3.68	5.20	3.67	<u>4.43</u>
28	22.1	56min	349	505	567	513	517	<b>525</b>	5.20	3.64	5.27	3.28	4.35

Table 15. Comparison of number of interaction blocks for IS2RE with auxiliary IS2RS. Scalability is measured with training time for one epoch (Train, in minutes) and inference throughput (Infer., number of samples processed in a second). Here the canonicalization technique is SE(3)-SFA, the number of warmup steps is 192000 (about half total number of steps), and the batch size is 64. Best score is in bold, second best score is underlined.

### C.5.3. CANONICALIZATION COMPARISON

We use SE(3)-SFA because it is less equivariant to reflections than Stochastic FA (which samples a frame in E(3)), but it has to learn data symmetries from fewer frames, which helps training. For both SE(3)-SFA and No-FA models, we observe in Table 16 that the equivariance-invariance do not seem to be correlated to the number of interaction layers. Moreover, we do not observe a clear correlation between the Average energy MAE and the equivariance-invariance.

When using SE(3)-SFA, we see a clear correlation between the increase in the number of interaction layers and the performances. In the No-FA case, the impossibility to learn equivariance and invariance even when adding more layers to the model might account for the less clear positive correlation between the performances (in terms of energy MAE) and the number of interaction layers than when we were applying SE(3)-SFA.

Canonicalization	Interactions	2D E-RI ↓	2D E-Ref-I ↓	2D Pos-RI ↓	2D Pos-Ref-I ↓	Average E-MAE (meV) ↓
SE(3)-SFA	5	22.7	34.7	55.0	80.3	546
SE(3)-SFA	14	29.7	43.2	61.7	90.4	537
SE(3)-SFA	16	21.4	33.6	56.0	83.4	<u>529</u>
SE(3)-SFA	18	19.0	30.2	53.9	78.4	544
SE(3)-SFA	20	22.6	34.7	56.2	82.8	542
SE(3)-SFA	22	20.8	32.6	56.3	81.7	530
SE(3)-SFA	28	25.5	37.3	60.8	86.5	<b>525</b>
SE(3)-SFA no aux	5	6.9	8.9			569
No-FA	8	111	107	253	238	<u>561</u>
No-FA	10	110	107	251	233	577
No-FA	14	121	117	275	254	562
No-FA	18	115	111	273	257	608
No-FA	22	116	111	260	240	<b>554</b>
No-FA	26	120	117	288	271	579

Table 16. Comparison of using SE(3)-SFA on both the energy and position prediction heads to No FA and to the top configs of FAENet with no auxiliary task from (Duval et al., 2023). The symmetry-preservation metrics are in meV for the energy and milli-Angstroms for the positions. The best model for each of the 2 categories is in bold and the second best is underlined. We do not seem to have a correlation between the quality of the invariance and equivariance with the number of interaction layers in both categories.

### C.6. Pre-training on different tasks

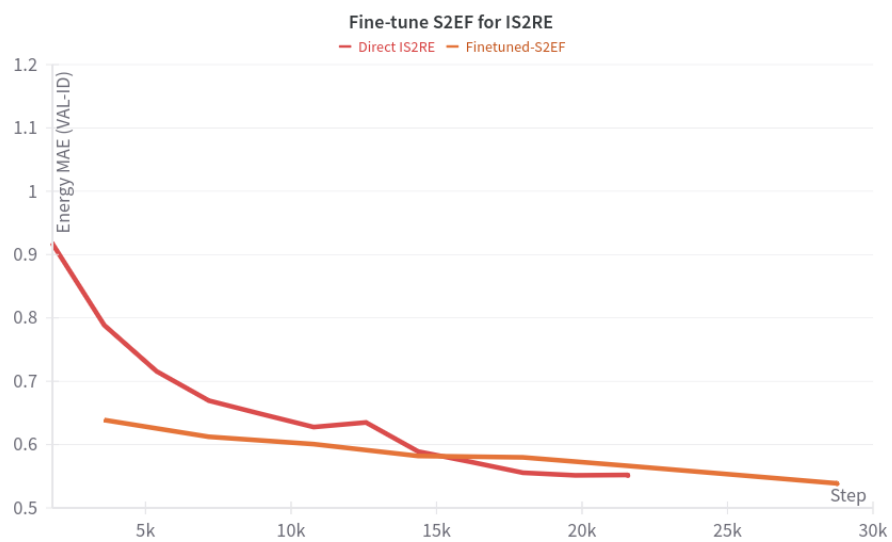


Figure 7. Validation curve during training for both a model trained directly from scratch for IS2RE and an S2EF model fine-tuned on IS2RE